Dalton Transactions

Redox-enhanced hemilability of the tris(tert-butoxy)siloxy ligand at cerium

Journal:	*Dalton Transactions*
Manuscript ID	DT-ART-05-2018-001878.R1
Article Type:	Paper
Date Submitted by the Author:	28-Jun-2018
Complete List of Authors:	Friedrich, Jochen; Eberhard Karls Universitat Tubingen, Qiao, Yusen; University of Pennsylvania Maichle-moessmer, Caecilia; Eberhard Karls Universität Tübingen Schelter, Eric J; University of Pennsylvania, Department of Chemistry Anwander, Reiner; Universitat Tubingen, Institut fur Anorganische Chemie

Journal Name

ARTICLE

Redox-enhanced hemilability of the tris(*tert*-butoxy)siloxy ligand at cerium†

Received 00th January 20xx,
Accepted 00th January 20xx

DOI: 10.1039/x0xx00000x

www.rsc.org/

Jochen Friedrich[a], Yusen Qiao[b], Cäcilia Maichle-Mössmer[a], Eric J. Schelter*[b] and Reiner Anwander*[a]

The stabilizing effect of the tris(*tert*-butoxy)silyoxy ligand on cerium(IV) is revealed by electrochemical and computation methods as well as targeted redox chemistry. Ceric homoleptic complex $Ce[OSi(OtBu)_3]_4$ was obtained by the reaction of $[Et_4N]_2[CeCl_6]$ with $NaOSi(OtBu)_3$ at ambient temperature in acetonitrile, while cerous ion-separated complex $[Ce\{OSi(OtBu)_3\}_4][K(2.2.2\text{-crypt})]$ was readily synthesized from $[Ce\{OSi(OtBu)_3\}_4K]$ and cryptand. The solid-state structures of monocerium complexes $Ce[OSi(OtBu)_3]_4$ and $Ce[OSi(OtBu)_3]_4(THF)$ show 5- and 6-coordinate Ce^{IV} centers (one κ^2-bonded siloxy ligand), while complex $[Ce\{OSi(OtBu)_3\}_4][K(2.2.2\text{-crypt})]$ exhibits a 4-coordinate Ce^{III} center (all-terminal siloxy coordination). A comparative electrochemical study of $Ce[OSi(OtBu)_3]_4$ and $[Ce\{OSi(OtBu)_3\}_4][K(2.2.2\text{-crypt})]$ suggests a redox-modulated molecular rearrangement process, featuring an oxidation-state dependent formation and release of a Ce---O*t*Bu coordination. While the overall stabilization of Ce^{IV} by the siloxy ligand is evident, significant extra stabilization is gained if the siloxy ligand coordinates in a chelating fashion, which is further supported by DFT calculations. Natural bond orbital (NBO) analysis indicates an enhanced donation of the siloxy ligand electron density into the unfilled Ce^{IV} 6s, 4f, and 5d orbitals. Ce^{IV} to Ce^{III} reduction readily occurs when homoleptic complex $Ce[OSi(OtBu)_3]_4$ is treated with cobaltocene, affording the separated ion pair $[Ce\{OSi(OtBu)_3\}_4][CoCp_2]$, featuring exclusive terminal siloxy bonding in the solid-state, similar to that detected for $[Ce\{OSi(OtBu)_3\}_4][K(2.2.2\text{-crypt})]$.

Introduction

Molecular electrochemistry has emerged as a powerful tool for analysing redox-active cerium compounds.[1,2] Various metalorganic Ce^{IV} complexes featuring Ce–O and Ce–N bonding were shown to exhibit well-defined reversible or quasi-reversible electrochemical behaviour.[1,3-14] Metal-ligand rearrangement processes were found as determining factors,[15,16] and more recently, a general focus was put on the oxidative and reductive occurrences at the Ce^{III} and Ce^{IV} ions, respectively. A diverse set of cerium ate complexes as well as cerium complexes with outer-sphere coordinated cations were included in these studies.[17-22] While most examples involved a weakly coordinated anion like, e.g., $[B(ArF)_4]^-$, the presence of donor solvent molecules or macrocycle-separated alkali-metal cations were also targeted.[2,15,16,20,23-34] More specifically, comparative electrochemical investigations of complexes $[Ce(TriNO_x)X]$ (X= $B(ArF)_4$, F, Cl, Br, I) and $[Ce\{N(SiMe_3)_2\}_3X]$ (X= F, Cl, Br), as well as $[\{Li_3(DMEDA)_3\}\{(BINOLate)_3CeX\}]$ (X= Cl, Br, I) revealed a dependence of the reversible behaviour on ion pair formation (presence of outer-sphere anions).[16,24,35] The extent and trend of the effect was found to be correlated with the bond strength and type of ancillary ligand, as well as complex stability. However, such cationic outer-sphere bonded cerium model complexes did not necessarily result in reversible redox features, partly ascribed to solvent effects.[23,36,37] Homoleptic complexes such as $[Ce\{tBuC(O)N(O)Ph\}_4]$,[38] $[Ce\{N(SiHMe_2)_2\}_4]$,[39] $[Ce\{ON(tBu)(2\text{-}OMe\text{-}5tBu\text{-}C_6H_3)\}_4]$,[40] and $[Ce\{C(Ph_2PNSiMe_3)_2\}_2]$[41] studied previously did not exhibit a completely reversible electrochemical behaviour, also attributed to rearrangement processes.[15,24,38-42]

It is plausible that the implementation of well-defined homoleptic Ce^{III} and alkali-metal-containing ate complexes,[15,16,39,43-48] was inevitable for gaining detailed knowledge about oxidative pathways and hence for advancing cerium chemistry. Along this line, inorganic Ce^{IV} salts can display useful precursors in salt metathesis protocols.[49] Accordingly, Leung *et al.* introduced $[Et_4N]_2[CeCl_6]$ as a suitable reagent for the synthesis of a series of ceric complexes stabilized by the bulky chelating ligands $[N\{P(iPr)_2O\}_2]^-$ and $[Co(\eta^5\text{-}C_5H_5)\{P(O)(OEt)_2\}_3]^-$ (L^{OEt-}).[50-52] This prompted us to investigate the reactivity of $[Et_4N]_2[CeCl_6]$ toward $NaOSi(OtBu)_3$, aiming at the homoleptic ceric tris(*tert*-butoxy)siloxide complex $Ce[OSi(OtBu)_3]_4$ (**1**, Chart 1) recently reported by us and others using Ce^{III}/Ce^{IV} redox protocols.[32,53] In the solid state, the monometallic Ce^{IV} complex **1** revealed a κ^2-coordination of one of the siloxy ligands (Chart 1), similar to the uranium siloxide complex $U[OSi(OtBu)_3]_4$.[53,55] Relevant tris(*tert*-butoxy)siloxide

[a] J. Friedrich, C. Maichle-Mössmer and R. Anwander; Institut für Anorganische Chemie; Eberhard Karls Universität Tübingen, Auf der Morgenstelle 18, 72076 Tübingen, Germany; E-mail reiner.anwander@uni-tuebingen.de.
[b] Y. Qiao and E. J. Schelter; P. Roy and Diana T. Vagelos Laboratories, Department of Chemistry, University of Pennsylvania; 231 S. 34th Street, Philadelphia, PA 19104, USA; E-mail schelter@sas.upenn.edu.

† Electronic Supplementary Information (ESI) available: Experimental details, NMR and FTIR spectroscopy, Cyclic voltammetry and Computational Data. CCDC 1826883 - 1826886. For ESI and crystallographic data in CIF or other electronic format see DOI: 10.1039/x0xx00000x

derivatives of the trivalent rare-earth elements (and cerium(III) in particular) have been isolated and characterized as ate complexes (Chart 1, **2**), silanol adducts (**A**) and dimeric homoleptic complexes (**B**).[53,54,56]

Chart 1. Distinct bonding modes in Ce^{IV} and Ce^{III} tris(*tert*-butoxy)siloxide complexes **1**,[53] **2**,[32] **A**[54] and **B**[53] as revealed from X-ray structure analysis.

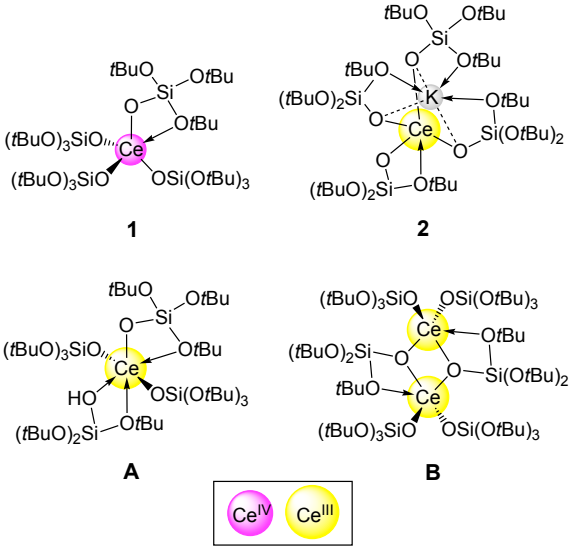

The $[OSi(OtBu)_3]^-$ ligand does not only engage in distinct coordination modes but also exhibits favourable electronic properties, which have been routinely exploited in transition metal chemistry.[57,58] In f-element chemistry, the tris(tert-butoxy)siloxy moiety gave access to distinct oxidation states of uranium (III, IV, V),[55,59] as well as of the lanthanides samarium (II, III), europium (II, III), ytterbium (II, III) and cerium (II, III, IV).[32,60] Cyclic voltammetry studies indicated high reducing properties of U^{IV}, Sm^{II}, Eu^{II} and Yb^{II} siloxide complexes, which were attributed to the inherent electronic character of this very siloxy ligand.[55,60] Despite electrochemical investigations of cerium siloxide complexes $[Ce(L^{OEt})(OSiPh_3)_3]$[14] and $[Ce(OSiMe_3)\{N(SiMe_3)_2\}_3\{Li(2.2.2\text{-crypt})\}]$,[29] studies involving the tris(*tert*-butoxy)siloxy ligand were not yet reported.

Given the recent isolation of $Ce[OSi(OtBu)_3]_4$ (**1**) we have now devoted efforts into evaluating any stabilizing effect of such siloxy environments at tetravalent cerium, giving consideration to supplementing experimental, electrochemical, and computational studies.

Results and discussion

Synthesis and characterisation of tetravalent $Ce[OSi(OtBu)_3]_4$. The reaction between $[Et_4N]_2[CeCl_6]$ and 4 equiv of $NaOSi(OtBu)_3$ was performed at ambient temperature in acetonitrile, employing conditions as reported by Leung.[50,51] Surprisingly, subsequent workup allowed the straightforward isolation of the homoleptic donor-free complex $Ce[OSi(OtBu)_3]_4$ (**1**) in moderate yield, as a clear improvement of our previously applied oxidation protocol utilizing **B** and Ph_3CCl (17% cryst.).[53] For further comparison, the oxidative approach described by Mazzanti *et al.* employing trivalent **2** and AgOTf as well as a considerably smaller batch size gave 63% of **1**.[32] With reasonable amounts of **1** in hand, we envisioned its more detailed characterization. Since the solid-state structure of **1** features two distinct siloxy coordination modes (see Chart 1, Scheme 1: three terminal and one chelating),[53] we were interested in the solution structure of **1**. More specifically, the effect of temperature and donor solvents on the κ^2-bonding mode might be significant. VT ^1H NMR spectroscopy experiments in CD_2Cl_2, $[D_8]$toluene and $[D_8]$THF did merely display signal broadening with decreasing temperatures, suggesting a highly fluxional coordination of the siloxy ligand not only in donor solvents, even at -60 °C (Figure S1-S3).

Crystallization attempts performed at -40 °C from a saturated solution of **1** in THF produced single-crystalline material suitable for X-ray diffraction analysis. The solid-state structure of $Ce[OSi(OtBu)_3]_4(THF)$ (**1(THF)**) revealed the presence of two independent molecules in the unit cell. The cerium atoms are 6-coordinate (Figure 1) with the THF molecule (Ce–O34/O17 2.520(13)/2.573(14) Å, molecule 1/2)) *trans*-positioned to a non-chelating siloxy ligand (O26–Ce2–O34 176.7(3) °). Even though, one κ^2-siloxy moiety is detectable, it shows Ce---O*t*Bu(donor) distances of 2.681(8) (molecule 1) and 2.729(8) Å (molecule 2), markedly elongated compared to donor-free 1 (Ce---O*t*Bu 2.593(2) Å).[53] The terminal Ce–O(siloxy) bond lengths in **1(THF)** range from 2.098(8) to 2.146(8) Å, and are 2.179(8)/2.203(8) Å for the κ^2-bonded siloxy moiety, all slightly elongated when compared to 5-coordinate **1**.[53]

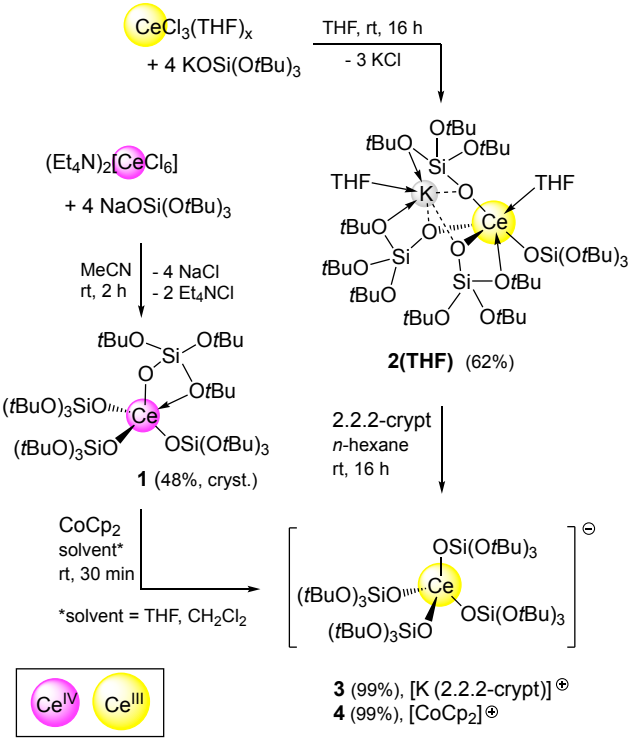

Scheme 1. Synthesis of Ce^{IV} and Ce^{III} siloxide complexes $Ce[OSi(OtBu)_3]_4$ (**1**), $[Ce\{OSi(OtBu)_3\}_4K](THF)_2$ (**2(THF)**), $[Ce\{OSi(OtBu)_3\}_4][K(2.2.2\text{-crypt})]$ (**3**) and $[Ce\{OSi(OtBu)_3\}_4][CoCp_2]$ (**4**).

Synthesis and characterisation of cerous tris(*tert*-butoxy)silyoxide complexes.

For a thorough electrochemical analysis of compound **1**, comparison was sought with a Ce^{III} model complex with similar ligand environment. THF-coordinated potassium ate complex [Ce{OSi(O*t*Bu)$_3$}$_4$(THF)K(THF)] (**2(THF)**) was initially envisaged as a suitable candidate. Complex **2(THF)** was obtained by salt-metathetic treatment of $CeCl_3$(THF) with KOSi(O*t*Bu)$_3$ in THF (Scheme 1), similarly to previously reported [Ce{OSi(O*t*Bu)$_3$}$_4$K] (**2**).[32] Skipping tedious work-up procedures, immediate crystallization from THF solution allowed the isolation of **2(THF)** in good yields. However, evaporation to dryness resulted in complete donor (THF) displacement affording analytically pure **2**. An X-ray diffraction analysis of single-crystalline **2(THF)** revealed the presence of a siloxy-incorporated potassium ion and a donor solvent-coordinated cerium ion (Figure 2). Similar structural motifs were described in ate complexes [Pb{OSi(O*t*Bu)$_3$}$_3$Na] and [Sn{OSi(O*t*Bu)$_3$}$_3$K],[61] [Ln{OSi(O*t*Bu)$_3$}$_4$K] (Ln= Sm, Eu, Yb)[60] and [Cr{OSi(O*t*Bu)$_3$}$_4$K].[62] However, the incorporation of donor solvent (THF) in complex **2(THF)**, results in elongated metal---alkoxy contacts (Na/K---O*t*Bu, M---O*t*Bu).

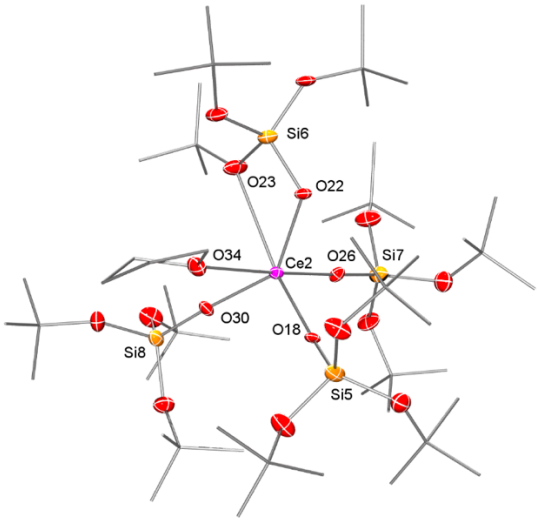

Figure 1. ORTEP representation of the molecular structure of Ce[OSi(O*t*Bu)$_3$]$_4$(THF) (**1(THF)**) with atomic displacement ellipsoids set at the 30% level; hydrogen atoms omitted for clarity; see ESI for a representation of the asymmetric unit; selected bond lengths [Å] and angles [°]: Ce2–O18 2.098(8), Ce2–O22 2.179(8), Ce2–O23 2.729(8), Ce2–O26 2.125(12), Ce2–O30 2.140(8), Ce2–O34 2.520(13), O18–Si5 1.652(9), O22–Si6 1.591(9), O26–Si7 1.601(12), O30–Si8 1.603(9), O18–Ce2–O22 100.3(3), O18–Ce2–O26 99.1(3), O18–Ce2–O34 84.2(3), O22–Ce2–O26 100.6(3), O22–Ce2–O30 141.7(3), O26–Ce2–O34 176.7(3), O30–Ce2–O34 79.5(3).

It should be noted that ate complexes comprising outer sphere-encapsulated cations were successfully employed in electrochemical analysis.[20,25,8,29,55,63] In order to achieve potassium/siloxy separation, a solution of **2** in THF/n-hexane (1:1) was treated with 1 equiv of 2.2.2-cryptand, yielding quantitatively single-crystalline [Ce{OSi(O*t*Bu)$_3$}$_4$][K(2.2.2-crypt)] (**3**). The generation of **3** was further evidenced by elemental analysis and ambient temperature ^{1}H NMR spectroscopy in [D$_8$]THF, which displayed one paramagnetically broadened resonance (1.08 ppm) shifted to lower field in comparison with **2**. X-ray diffraction analysis of complex **3** revealed a distorted tetrahedral geometry of the cerium centre without a κ^2-siloxy moiety and an outer sphere-encapsulated potassium ion (Figure 3). Complex **3** is isostructural with the U^{III} congener [U{OSi(O*t*Bu)$_3$}$_4$][K(2.2.2-crypt)].[59] As a result of the lower coordination number, the Ce–O distances (2.207(5)-2.236(4) Å) in complex **3** are shorter than found for the terminal siloxy ligands in 6-coordinate complex **2(THF)** (Ce–O$_{terminal}$ 2.293(3) Å).

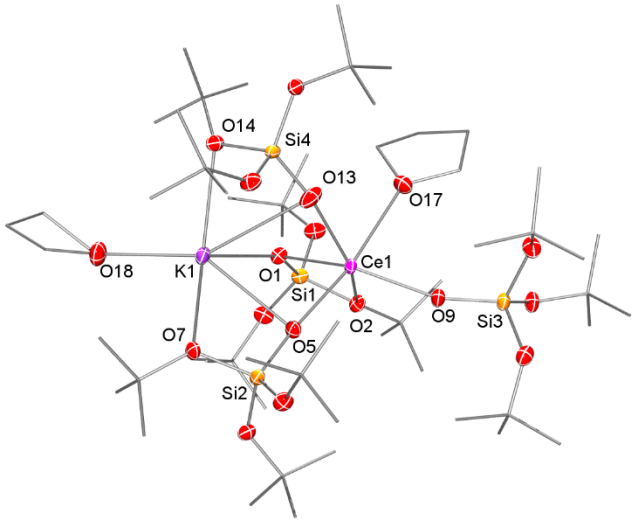

Figure 2. ORTEP representation of the molecular structure of [Ce{OSi(O*t*Bu)$_3$}$_4$(THF)K(THF)] (**2(THF)**) with atomic displacement ellipsoids set at the 30% level; hydrogen atoms are omitted for clarity. Selected bond lengths [Å] and angles [°]: Ce1–O1 2.3994(12), Ce1–O2 2.7463(12), Ce1–O5 2.2807(11), Ce1–O9 2.293(3), Ce1–O13 2.2876(13), Ce1–O17 2.6228(12), O1–Si1 1.5804(12), O5–Si2 1.5854(12), O9–Si3 1.589(3), O13–Si4 1.517(4), K1–O1 2.6210(12), K1–O5 2.9104(13), K1–O7 2.8178(12), K1–O13 3.1181(14), K1–O14 2.807(4), K1–O18 2.7609(14), O1–Ce1–O5 85.53(4), O1–Ce1–O9 148.99(7), O1–Ce1–O13 89.10(4), O5–Ce1–O9 103.73(7), O5–Ce1–O13 88.78(5), O5–Ce1–O17 170.98(4), O1–K1–O18 114.81(4), O5–K1–O18 143.49(4), O13–K1–O18 152.59(4).

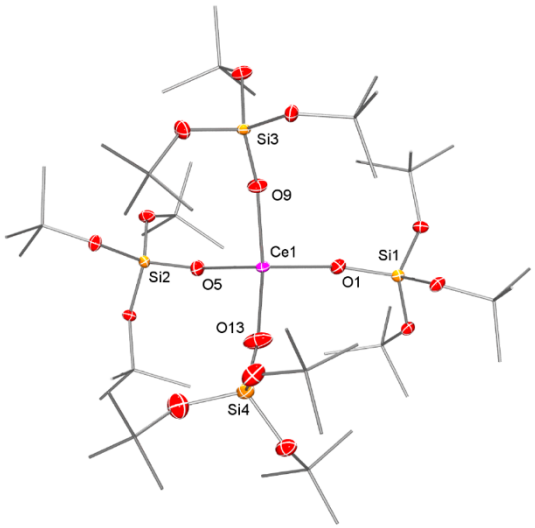

Figure 3. ORTEP representation of the molecular structure of [Ce{OSi(O*t*Bu)$_3$}$_4$][K(2.2.2-crypt)] (**3**) with atomic displacement ellipsoids set at the 30% level; hydrogen atoms are omitted for clarity; see ESI for a representation of the asymmetric unit. Selected bond lengths [Å] and angles [°]: Ce1–O1 2.236(4), Ce1–O5 2.207(5), Ce1–O9 2.232(4), Ce1–O13 2.215(5), O1–Si1 1.579(5), O5–Si2 1.594(5), O9–Si3 1.589(4), O13–Si4 1.570(5), O1–Ce1–O5 103.31(17), O1–Ce1–O9 109.25(17), O1–Ce1–O13 112.85(19), O5–Ce1–O9 108.38(17), O5–Ce1–O13 111.5(2), O9–Ce1–O13 111.21(17).

Electrochemical investigation of the Ce^{IV}/Ce^{III} tris(*tert*-butoxy)silyoxide complexes.

Cyclic voltammetry (CV) experiments of complexes **1** – **3** were conducted at ambient temperature (26°C) in CH_2Cl_2, THF and DME solutions, containing 0.1 M of $[nPr_4N][B\{Ar(3,5\text{-}CF_3)\}_4]$ as supporting electrolyte. The obtained current-potential curves were characterized by electrochemically irreversible anodic and cathodic redox features as well as wide peak separations (Figure 4, ΔE~ 1.2 V; Table 1). Such behaviours have been previously ascribed to a high kinetic barrier for electron transfer and molecular rearrangement, as well as over potential,[1,64,65] with ion-pair formation as a proven cause.[23,24,36]

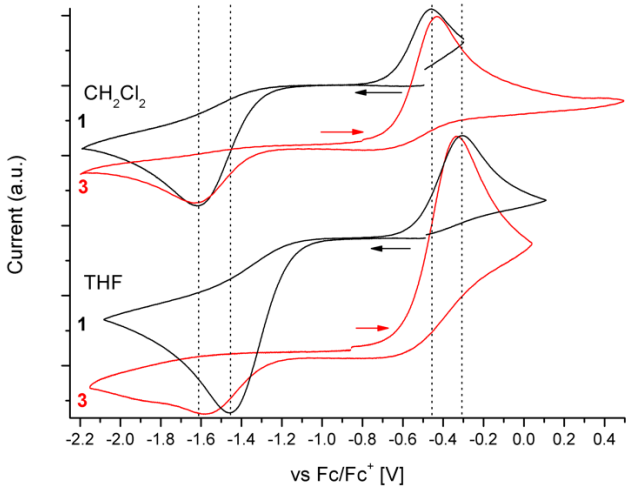

Figure 4. Influence of donor solvent on the Ce(III/IV) redox couples of complexes $Ce[OSi(OtBu)_3]_4$ (**1**, black trace) and $[Ce\{OSi(OtBu)_3\}_4][K(2.2.2\text{-crypt})]$ (**3**, red trace) obtained at 250 mV/s scan rates; arrows indicate the scan direction; *c*(analyte) ~1 mM, *c*(electrolyte) 0.1 M $[nPr_4N][B\{Ar(3,5\text{-}CF_3)\}_4]$.

Table 1. Electrochemical data of complexes 1 and 3 in selected solvents (Figure 4).

	complex	E_{pc} [V vs Fc]	E_{pa} [V vs Fc]	ΔE [V]
CH_2Cl_2[a]	**1**[c]	-1.61	-0.46	1.15
	2[d]	-1.09	+0.33	1.42
	3[c]	-1.64	-0.43	1.20
THF[a]	**1**[c]	-1.46	-0.31	1.15
	2[d]	-1.53	-0.20	1.34
	3[c]	-1.58	-0.33	1.25
DME[a]	**1**[d]	-1.43	-0.31	1.12
THF[b]	**1**[d]	-1.60	-0.23	1.37
DME[b]	**1**[d]	-1.50	-0.20	1.30

[a] 26 °C, [b] -20 °C, [c] see Figure 4, [d] see ESI.

Notwithstanding, similar potential values for the reductive (E_{pc}~ -1.6 V) and oxidative (E_{pa}~ -0.4 V) responses were measured in CH_2Cl_2 solvent for complexes **1** (black trace, Figure 4) and **3** (blue trace), indicating their electrochemical mutual interconversion according to ECEC processes (Electron Transfer followed from Chemical Reaction, e.g. hemilability of the κ^2-coordination), resulting in a square scheme. Interestingly, also closely analogous CV waves were reported for redox-stimulated isomerization reactions of ruthenium complexes containing ambidentate polypyridyl ligands.[66] The latter observation was explained by a fast isomerization reaction or ligand rearrangement following oxidative electron transfer. Based on the kinetic facts an irreversible CV wave was observed. Subsequently, the reductive response of the generated species was detected at a negatively shifted potential, being far-separated from the oxidative wave. However, the cathodic feature had also an irreversible appearance, if isomerization or rearrangement proceeded under regeneration of the initial molecule.[66]

For the present case, we suggest a similar scenario on the electrochemical timescale (Scheme 2). We propose that reduction of complex **1** gives the trivalent intermediate species Int1 with an intact κ^2-bonded siloxy moiety. Switching the oxidation state from Ce^{IV} to Ce^{III} implicates an increased ionic radius (Δ~ 0.1 Å),[67] resulting in decreased Lewis acidity of the rare-earth metal centre and hence a changed HSAB coordination preference.[68-70] Consequently, intermediate Int1 can undergo fast rearrangement ($k1_{rear.}$) involving a coordination switch of the siloxy ligand from κ^2 to terminal as found in model complex **3**.

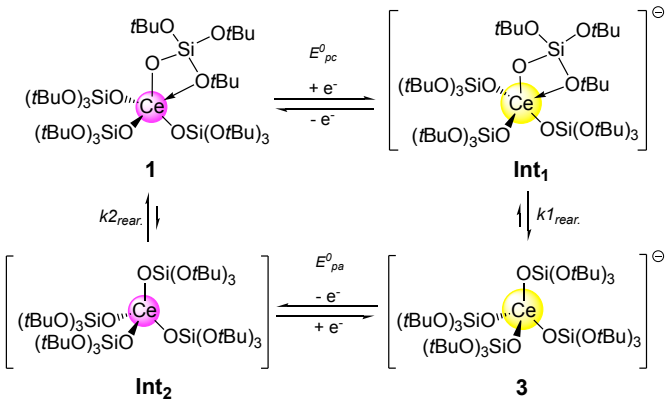

Scheme 2. Proposed scenario for the electrochemical stimulation of the oxidation-state dependent formation/release of the hemi labile κ^2-bonding of the Ce---O*t*Bu moiety.

As a result, no oxidative return wave was observed next to the reductive feature (E_{pc}= -1.61 V) in the cyclic voltammogram. Instead, a response wave was detected corresponding to the oxidation of a new species similar to complex **3** (E_{pa}= -0.46 V). Compatible with this, oxidation of **3** resulted in the generation of the tetravalent intermediate species **Int_2**, which upon the reverse coordination switch converts further into siloxide complex **1** ($k2_{rear.}$). Obviously, the combination of tris(*tert*-butoxy)siloxy ligands including additional coordination of the O*t*Bu moiety resulted in a significant stabilization of the Ce^{IV} oxidation state (E_{pc}= -1.61 V; ΔE= 1.15 V) versus the Ce^{III} ion at E_{pa}= -0.46 V.

In accordance with this, the X-ray structure analysis of complex **1(THF)** displays an elongated κ^2-bonding of the siloxy ligand in the solid state in comparison with the donor-free congener (vide supra).[53] As a result of the seemingly less pronounced stabilization of Ce^{IV} ion, slightly anodic-shifted (ΔE_{pc}~ +0.15 V;

Table 1) CV current-potential curves were observed for complex **1** in THF (red trace; Figure 4) and DME solvent (Figure S16). However, measurement of complex **3** in THF (green trace) did not strictly follow the electrochemical appearance of **1**, possibly caused by differing kinetics (generation of **1** from **Int$_2$**). Also, low-temperature CV experiments of complex **1** in donor solvents THF and DME at -20°C provided further support for the proposed scenario. Both measurements exhibited farther separated anodic and cathodic redox features (ΔE~ 1.30 V; see ESI Figure S22-S23), which can be explained by slower ligand rearrangement processes (Scheme 2: $k1_{rear.}$ and $k2_{rear.}$). The less emphasized peak separation in DME most likely originates from a slightly changed coordination sphere (Table 1). Unfortunately, we could not obtain a single crystalline material of putative complex **1(DME)**.

Chemical reduction of Ce[OSi(O*t*Bu)$_3$]$_4$ with cobaltocene.

Chemical screening of the reduction reaction and possible follow-up reactions seemed a viable approach to further substantiate our hypothesis concerning the CV observations. To this end, reduction of complex **1** with a suitable reagent seemed feasible. According to Connelly and Geiger,[36] a series of reductants are capable of a one-electron reduction of distinct Ce^{IV} complexes. We chose cobaltocene (THF: -1.46 V vs Fc/Fc$^+$) since it was previously successfully implemented in cerium redox chemistry.[36,71,72] Monitoring the addition of increasing equivalents of $CoCp_2$ (0.2-1 equiv) to a [D$_8$]THF solution of **1** (see Figure S9, NMR-scale experiment), allowed a more detailed understanding of the electrochemical observations.[36] The ambient temperature ^{1}H NMR spectrum displayed distinct signals of reduction product [Ce{OSi(O*t*Bu)$_3$}$_4$][$CoCp_2$] (**4**) (5.86 (C_5H_5), 1.07 ppm, 108H, ($C(CH_3)_3$)), of which the *t*Bu proton resonances were coinciding with the respective ones of **3** (Figures S6 and S8). However, the signals of **4** were accompanied by low intensity but clearly assignable resonances of the paramagnetic complex [Ce{OSi(O*t*Bu)$_3$}$_3$]$_2$ (**B**, Chart 1)[53] and proligand HOSi(O*t*Bu)$_3$. Further undefined side-products were also generated in minor amounts. Trivalent complex [Ce{OSi(O*t*Bu)$_3$}$_4$][$CoCp_2$] (**4**) (Scheme 2) could be obtained quantitatively by treatment of complex **1** with stoichiometric amounts of $CoCp_2$ in CH_2Cl_2 or THF solutions. From both experiments, single-crystalline material suitable for X-ray diffraction analysis could be easily harvested at -40°C in saturated solutions of toluene. The structural motive of complex **4** found in the solid state shows again a separated ion pair with a 4-coordinate cerium ion (Figure 5), closely resembling complex **3**. The Ce–O distances in **4** (2.220(2)-2.267(2) Å) appeared marginally elongated, but match those observed in complex **3** (2.207(5)-2.236(4) Å). Generation of **4** was further supported by elemental analysis and IR spectroscopy.

The ambient temperature ^{1}H NMR spectrum of pure complex **4** in [D$_8$]THF displayed paramagnetically broadened resonances of the Cp (5.16 ppm; Figure S8) and *t*Bu protons (1.07 ppm), in accordance with the trivalent species observed in the NMR experiment vide supra. A similar shift was observed in complex **3** comprising the outer sphere-encapsulated potassium ion (Figure S7), further corroborating the presence of outer sphere coordinated ions in THF solutions of complexes **3** and **4**. However, once more the solution instability of **4** is emphasized by a weak signal assignable to [Ce{OSi(O*t*Bu)$_3$}$_3$]$_2$ (**B**, Chart 1).[53]

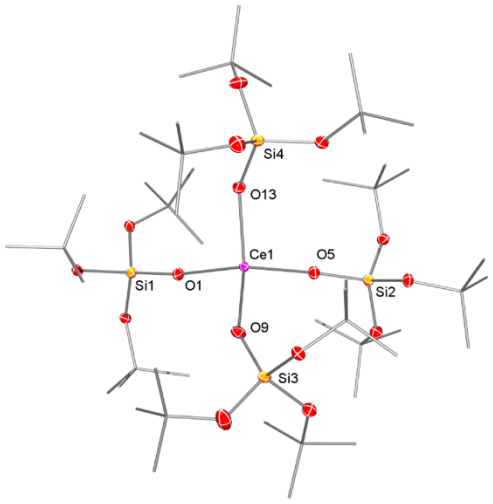

Figure 5. ORTEP representation of the molecular structure of [Ce{OSi(O*t*Bu)$_3$}$_4$][$CoCp_2$] (**4**) with atomic displacement ellipsoids set at the 30% level; hydrogen atoms are omitted for clarity; Selected bond lengths [Å] and angles [°]: Ce–O1 2.267(2), Ce–O5 2.220(2), Ce–O9 2.253(2), Ce–O13 2.249(2), O1–Si1 1.587(2), O5–Si2 1.589(2), O9–Si3 1.583(2), O13–Si4 1.590(2), O1–Ce–O5 108.99(8), O1–Ce–O9 106.91(9), O1–Ce–O13 106.34(8), O5–Ce–O9 110.77(9), O5–Ce–O13 109.23(8), O9–Ce–O13 114.38(9).

DFT calculations.

To further explore the role of the additional coordination of the O*t*Bu moiety in the stabilization of the Ce^{IV} oxidation state of **1**, we computed the electronic structures of **1** and **3** by DFT calculations. The optimized structures were in good agreement with the crystallographically determined bond lengths and bond angles (Tables S11 and S14). In addition, the trivalent intermediate species **Int$_1$** and tetravalent intermediate species **Int$_2$** (Scheme 2) were also computed for comparison between the electronic structures with and without the κ^2-coordination mode of the siloxy ligand. These calculations were performed using the crystal structure of **1** and **3**, respectively, as the starting points. In the Ce^{IV} oxidation state of **1** and **Int$_2$**, the highest occupied molecular orbital (HOMO) has primarily ligand AO character (99.1 %) and negligible Ce AO character (0.9 %) (Figure 6). Major contribution from Ce 4f character (97.4 %) was found in the lowest unoccupied molecular orbital (LUMO) of **1** and **Int$_2$** (Figure 6).

Unlike the Ce^{IV} oxidation state of **1** and **Int$_2$**, the HOMO of **Int$_1$** and **3** had primarily Ce 4f character (98.1%) and negligible 5d character (0.6%) (Figure 6). The HOMO energy of **Int$_1$** (-4.08 eV) was slightly higher than that of **3** (-4.12 eV), indicative of the lower Ce$^{III/IV}$ reduction potential in **Int$_1$**.[73] This result potentially revealed the stabilization of Ce^{IV} oxidation state by the additional coordination of the O*t*Bu moiety, consistent with the experimental electrochemical data. The HOMO-1 of **Int$_1$** and **3** were composed of primarily ligand AO character (98.8%). We next performed natural bond orbital (NBO) analyses for the Ce^{III} and Ce^{IV} siloxides to investigate the ligand to metal electron

donation affected by the κ^2-coordination mode of the siloxy ligand.

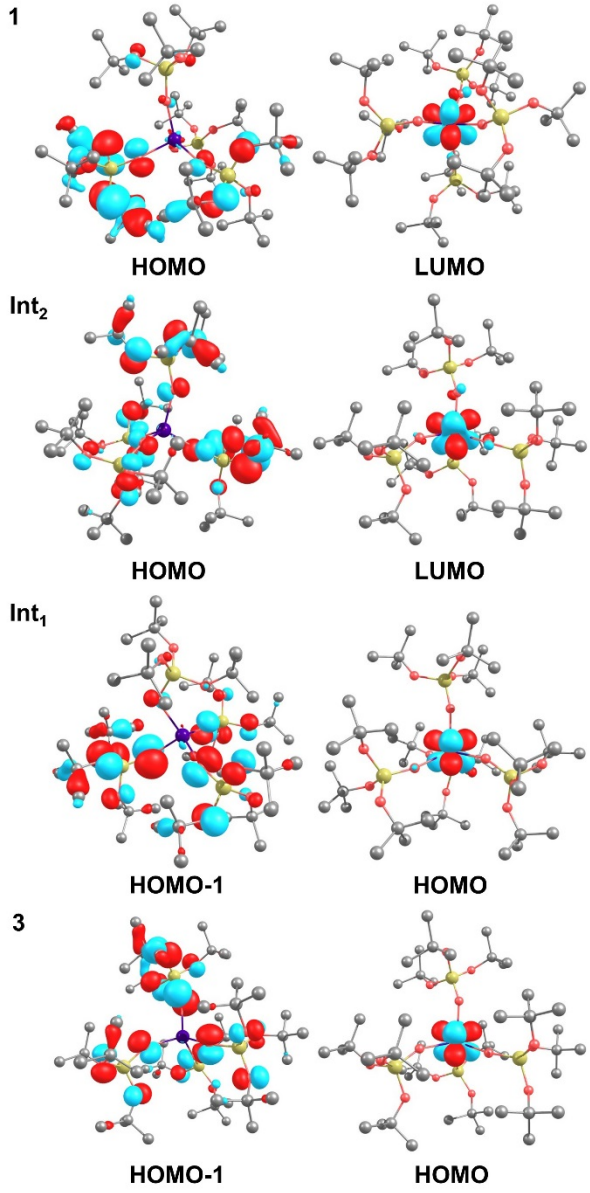

Figure 6. The Kohn–Sham orbitals of **1**, **Int$_2$**, **Int$_1$**, and **3**.

Atomic charges and orbital populations of the Ce centre for **1**, **Int$_2$**, **Int$_1$**, and **3** were computed by NBO charge and population analyses (Table 2). The calculated Ce natural charge (q_{Ce}) in **1** (2.31) was smaller than that in **Int$_2$** (2.40). Moreover, the sum of the Ce 6s, 4f and 5d populations was 1.69 electrons in **1** and decreased to 1.62 in **Int$_2$**. These results indicated a greater donation of the siloxy ligand electron density into the unfilled Ce 6s, 4f, and 5d orbitals for **1** due to the additional coordination of the O*t*Bu moiety in **1**. The difference of q_{Ce} and population sums between the trivalent **Int$_1$** and **3** was less profound compared to that of the tetravalent **1** and **Int$_2$** (Table 2). Overall, the DFT-computed results explained the extra stabilization of the Ce^{IV} oxidation state by the κ^2-coordination mode of one siloxy ligand.

Table 2. Natural charge (q_{Ce}) and natural population (6s, 5d, and 4f) of **1**, **Int$_2$**, **Int$_1$**, and **3**.

complex	q_{Ce}	Ce population	sum of Ce population
1	2.31	$6s^{0.06}4f^{0.68}5d^{0.95}$	1.69
Int$_2$	2.40	$6s^{0.06}4f^{0.65}5d^{0.91}$	1.62
Int$_1$	2.13	$6s^{0.06}4f^{1.11}5d^{0.68}$	1.85
3	2.18	$6s^{0.06}4f^{1.11}5d^{0.64}$	1.81

Conclusions

The ceric salt $[Et_4N]_2[CeCl_6]$ is an easy-to-handle precursor for homoleptic Ce^{IV} complex Ce[OSi(O*t*Bu)$_3$]$_4$. A combination of electrochemical and computational studies revealed the facile oxidizability of the Ce^{III} ion in the presence of this siloxy ligand. Accordingly, the higher Lewis-acidic, albeit naturally smaller, Ce^{IV} ion gains extra stabilization by exploiting κ^2-bonding of one the siloxy ligands, involving a peripheral O*t*Bu moiety. In the solid state this "weak" chelate coordination is not even abandoned in the presence of donor molecules as evidenced for the solid-state structure of Ce[OSi(O*t*Bu)$_3$]$_4$(THF). A comparative analysis of the Ce^{III} model complex [Ce{OSi(O*t*Bu)$_3$}$_4$][K(2.2.2-crypt)] further elucidated the redox-modulated formation and release of the Ce---O*t*Bu coordination. The hemilability of the tris(*tert*-butoxy)siloxy ligand was also revealed in the solid-sate structures of [Ce{OSi(O*t*Bu)$_3$}$_4$][K(2.2.2-crypt)] and [Ce{OSi(O*t*Bu)$_3$}$_4$][$CoCp_2$], showing an all-terminal bonding of the siloxy ligands. The latter cerous complex was obtained quantitatively by targeted reduction of homoleptic Ce[OSi(O*t*Bu)$_3$]$_4$ with cobaltocene. The entire redox-modulated ligand rearrangement scenario is also supported by DFT calculations. Enhanced donation of the siloxy ligand electron density into the unfilled Ce^{IV} orbitals is clearly indicated by natural bond orbital (NBO) analysis. Taking into consideration that the tris(*tert*-butoxy)siloxy ligand is a prominent model for a molecular silica surface, the present endeavour, aimed at a qualitative understanding of the Ce–OSiO*t*Bu coordination, might also contribute to a better assessment of the Ce–OSiO bonding in ceria-silica hybrid materials of relevance for redox catalysis.[74,75]

Experimental Section

General procedures

All operations were performed with rigorous exclusion of oxygen and moisture under an argon atmosphere. The syntheses were carried out either in a glovebox (MBraun MB200B; <1 ppm O_2, <1 ppm H_2O) or according to standard Schlenk techniques. Anhydrous $CeCl_3$ (99.99% trace metal basis), $KN(SiMe_3)_2$ (95%), HOSi(O*t*Bu)$_3$ (99.99% trace metal

basis) and 4,7,13,16,21,24-hexaoxa-1,10-diazabicyclo[8.8.8]hexacosane (98%) were purchased from Sigma-Aldrich and used as received. $CoCp_2$ was also purchased from Sigma-Aldrich and sublimed in vacuum before use. Anhydrous cerium(III) chloride (Sigma-Aldrich) was converted into $CeCl_3(THF)$ via Soxhlet extraction. $Ce[N(SiMe_3)_2]_3$,[76] $NaOSi(OtBu)_3$,[53] $KOSi(OtBu)_3$[32] and $[Et_4N]_2[CeCl_6]$[77] were synthesized according to literature procedures. Toluene, *n*-hexane, *n*-pentane, CH_2Cl_2 and THF were dried and degassed prior to use and provided by an MBraun SPS-800. C_6D_6, [D_8]toluene and [D_8]THF were obtained from Euriso-top, degassed, dried over NaK for at least 24 h, and filtered prior to use ([D_8]THF was distilled). CD_2Cl_2 was obtained from Euriso-top, degassed and dried over mole sieve 3 Å for at least 7 d. NMR spectra were recorded on a Bruker AVII+400 spectrometer. Infrared spectra were recorded on a Thermo Fisher Scientific NICOLET 6700 FTIR spectrometer using a DRIFT chamber with KBr windows. The samples were prepared in a glovebox and mixed with KBr powder. The collected data were refined by the Kubelka-Munk baseline correction. Elemental analyses were determined by an Elementar Vario Micro Cube.

Experimental details

Synthesis of $Ce[OSi(OtBu)_3]_4$ (**1**). $[Et_4N]_2[CeCl_6]$ (200 mg, 0.33 mmol) and $NaOSi(OtBu)_3$ (373.5 mg, 1.30 mmol) were stirred in acetonitrile for 2 h, causing a colour change of the suspension from initially orange to reddish. Subsequent centrifugation, separation of the supernatant and evaporation to dryness under vacuum left a red solid. Extraction with acetonitrile gave a reddish extract and left a pale reddish solid. Extraction of the residue with *n*-hexane allowed for the isolation of **1** which was recrystallized from THF to yield colourless analytically pure **1** (187 mg, 0.16 mmol, 48%). Detailed analysis of **1** was reported previously.[53]

Improved synthesis of $[Ce\{OSi(OtBu)_3\}_4K]$ (**2**).[32] A solution of $KOSi(OtBu)_3$ (500 mg, 1.65 mmol) in 3 mL THF was added to a suspension of $CeCl_3(THF)$ (131.6 mg, $4.13\cdot10^{-1}$ mmol) in 3 mL of THF. The colourless suspension was stirred for 16 h. A colourless solid was obtained from the supernatant after evaporation of the solvent. Subsequent extraction with n-hexane resulted in a colourless solid, which was recrystallized from THF to yield pure colourless product (315 mg, $2.55\cdot10^{-1}$ mmol, 62%). Crystals of **2(THF)** suitable for an X-ray diffraction analysis were grown at -40°C from a saturated solution in THF. ^{1}H NMR (400.13 MHz, C_6D_6, 26°C, TMS) δ [ppm]: 0.24 (s, 108H, $OSi[OC(CH_3)_3]_3$); (400.13 MHz, [D_8]THF, 26 °C, TMS) δ [ppm]: 0.34 (s, 108H, $OSi[OC(CH_3)_3]_3$); (400.13 MHz, CD_2Cl_2, 26°C, TMS) δ [ppm]: -0.03 (s, 108H, $OSi[OC(CH_3)_3]_3$). Elemental analysis calcd (%) for $C_{48}H_{108}CeKO_{16}Si_4$: C 46.76, H 8.83; found: C 46.77, H 8.88.

Synthesis of $[\{CeOSi(OtBu)_3\}_4\{K(2.2.2\text{-crypt})\}]$ (**3**). A solution of $[Ce\{OSiOtBu_3\}_4K]$ (100 mg, $8.11\cdot10^{-2}$ mmol) and 2.2.2-crypt (31.2 mg, $8.11\cdot10^{-2}$ mmol) in 8 mL of *n*-hexane/THF (1:1) was stirred overnight. After filtration and evaporation of the solvent **3** was obtained as a colourless powder (129.6 mg, $8.05\cdot10^{-2}$ mmol, 99%). Crystals suitable for X-ray diffraction were isolated after slow evaporation of the solvent. ^{1}H NMR (400.13 MHz, [D_8]THF, 26°C, TMS) δ [ppm]: 3.60 (s, 12H, CH_2 (2.2.2-crypt)), 3.56 (t, 12H, CH_2 (2.2.2-crypt)), 2.57 (t, 12H, CH_2 (2.2.2-crypt)), 1.08 (s, 108H, $OSi[OC(CH_3)_3]_3$); (400.13 MHz, CD_2Cl_2, 26°C, TMS) δ [ppm]: 3.59 (s, 12H, CH_2 (2.2.2-crypt)), 3.52 (t, 12H, CH_2 (2.2.2-crypt)), 2.54 (t, 12H, CH_2 (2.2.2-crypt)), 1.00 (s, 108H, $OSi[OC(CH_3)_3]_3$). Elemental analysis calcd (%) for $C_{66}H_{144}CeKN_2O_{22}Si_4$: C 49.26, H 9.02, N 1.74; found: C 49.22, H 8.99, N 1.79.

Synthesis of $[Ce\{OSi(OtBu)_3\}_4][CoCp_2]$ (**4**). $Ce[OSi(OtBu)_3]_4$ (40 mg, $3.35\cdot10^{-2}$ mmol) was dissolved in 1.5 mL of solvent (CH_2Cl_2 or THF). Dropwise addition of dissolved $CoCp_2$ (6.3 mg, $3.35\cdot10^{-2}$ mmol) (1.5 mL solvent; CH_2Cl_2 or THF) under stirring resulted in a yellow solution which was stirred for 30 min. Subsequent evaporation of the solvent and drying under vacuum left a yellow powder (using CH_2Cl_2: 47.3 mg, $3.32\cdot10^{-2}$ mmol, 94%; using THF: 43.5 mg, $3.14\cdot10^{-2}$ mmol, 99%). Crystals suitable for X-ray diffraction were grown from a saturated solution in toluene. ^{1}H NMR (400.13 MHz, [D_8]THF, 26°C, TMS) δ [ppm]: 5.16 (s (br), 10H, C_5H_5), 1.07 (s, 108H, $OSi[OC(CH_3)_3]_3$). Elemental analysis calcd (%) for $C_{58}H_{118}CeCoO_{16}Si_4$: C 50.37, H 8.60; found: C 50.82, H 8.45.

NMR-scale reaction of $Ce[OSi(OtBu)_3]_4$ (**1**) with $CoCp_2$ (Figure S8). $Ce[OSi(OtBu)_3]_4$ (9.3 mg, $7.79\cdot10^{-3}$ mmol) was dissolved in 0.5 mL of THF containing $O(SiMe_3)_2$ (4.9 mg, $3.02\cdot10^{-2}$ mmol) as an internal standard. $CoCp_2$ (0.295 mg, $1.56\cdot10^{-3}$ mmol) was dissolved in [D_8]THF and added in portions.

Electrochemical studies

Cyclic voltammetry (CV) experiments were performed with a Nordic Electrochemistry ECi-200 workstation applying the IR-compensation mode. The data were recorded using Nordic Electrochemistry EC4 DAQ software (version 4.1.90.1) and processed with EC-4 VIEW software (version 1.2.36.1). The CV experiments were conducted in a glovebox with argon atmosphere as described vide supra. The setup comprised a 4 mL glass vail, equipped with a CHI 104 glassy carbon disc working electrode (CH Instruments, Inc.), a platinum wire counter electrode, and a Ag/AgCl quasi reference electrode. The surface of the working electrodes was polished prior to each measurement. Solutions containing ~1 mM of analyte and 0.1 M $[nPr_4N][B\{Ar(3,5\text{-}CF_3)\}_4]$ supporting electrolyte were used for the electrochemical analyses. The scan rate dependent background of the electrolyte was recorded for each measurement and subtracted from the analyte data. The potentials are reported in [V] vs. the Fc/Fc^+ couple which was used as internal standard for cell calibration and determined at the end of each measurement.

Computational details

Gaussian 09 Rev. A.02 was used in electronic structure calculations.[78] The B3LYP hybrid DFT method was employed with 28-electron small core pseudopotentials on cerium with published segmented natural orbital basis sets incorporating quasi-relativistic effects,[79] and the 6-31G* basis set on all other atoms. All geometry optimizations were carried out starting from the coordinates of the crystal structures with the spin state restrained to doublet for Ce^{III} and singlet for Ce^{IV}. The geometry optimizations and frequency calculations were performed with

the conductor-like polarizable continuum model (CPCM)[80] with the Gaussian-defined solvent parameters for CH_2Cl_2. Frequency calculations of all calculated complexes found no negative frequencies, indicating the optimized structures found were at energy minima. Calculated metal-ligand bond lengths were within 0.07 Å of the crystal structures in all cases. Atomic orbital contributions to individual molecular orbitals were calculated with the AOMix program.[81,82] Molecular orbitals were rendered using Chemcraft v1.6 program.[83] Details of the various electronic states of interest, *e.g.* orbital occupations, electronic configurations, atomic charges, etc., were explored by natural bond orbital (NBO) population analyses.[84]

X-ray crystallography and crystal structure determinations

Suitable single crystals for X-ray structure analyses were selected in a glovebox and coated with Paratone-N HR2-643 and fixed on a nylon loop fibre. Data for compounds **3** and **4** were collected on a Bruker APEX DUO instrument equipped with an IμS microfocus sealed tube and QUAZAR optics for $Mo_{K\alpha}$ radiation (λ = 0.71073 Å). Data for compound **1(THF)** and **2** were collected on a Bruker SMART APEX II instrument equipped with a fine focus sealed tube and curved graphite monochromator using $Mo_{K\alpha}$ radiation (λ = 0.71073 Å). The data collection strategy was determined using COSMO[85] employing ω- and φ scans. Raw data were processed using APEX[86,87] and SAINT,[88,89] corrections for absorption effects were applied using SADABS.[90,91] The structures were solved by direct methods (SHELXS-1997/2013)[92] and refined against all data by full-matrix least-squares methods on F2 (SHELXL-1997/2014).[93] All graphics were produced employing ORTEP-3[94] and POV-Ray.[95] Further details of the refinement and crystallographic data are listed in Table 3 and in the CIF files. CCDC (**1(THF)**), (**2(THF)**), (**3**) and (**4**) contain the supplementary crystallographic data for this publication. These data can be obtained free of charge from The Cambridge Crystallographic Data Centre via www.ccdc.cam.ac.uk/data_request/cif.

Table 3. Crystallographic data for compounds **1(THF)**, **2(THF)**, **3** and **4**.

	1(THF)	**2(THF)**	**3**	**4**
CCDC	1826883	1826884	1826886	1826885
empirical formula	$(C_{52}H_{116}CeO_{17}Si_4)_2$ (C_4H_8O)	$C_{56}H_{124}CeKO_{18}Si_4$	$C_{66}H_{144}CeKN_2O_{22}Si_4$	$C_{58}H_{118}CeCoO_{16}Si_4(C_7H_8)_2$
M_w [g mol^{-1}]	1301.97	1377.12	1609.40	1567.19
T [K]	200(2)	100(2)	100(2)	100(2)
crystal system	trigonal	monoclinic	orthorhombic	monoclinic
space group	P 3_2	P $2_1/n$	P 2_1 2_1 2_1	P $2_1/c$
a [Å]	14.0472(3)	22.4960(9)	25.933(3)	20.536(4)
b [Å]	14.0472(3)	14.8753(4)	26.147(3)	16.007(3)
c [Å]	66.0924(14)	23.0312(7)	26.188(3)	25.726(5)
α [°]	90	90	90	90
β [°]	90	106.034(2)	90	91.04(3)
γ [°]	120	90	90	90
volume [Å^3]	11294.4(5)	7407.2(4)	17757(3)	8455(3)
Z	6	4	8	4
density (calculated) ρ [mg mm^{-3}]	1.149	1.235	1.204	1.231
absorption coefficient μ [mm^{-1}]	0.723	0.794	0.675	0.841
R1 (obs)[a]	0.0550	0.0282	0.0401	0.0422
wR2 (all)[b]	0.1154	0.0599	0.0896	0.0979
diffractometer	Bruker APEX II	Bruker APEX II	Bruker APEX DUO	Bruker APEX DUO

[a] Final R indices [I>2sigma(I)]; [b] R indices (all data)

Acknowledgements

We thank the German Science Foundation (Grant AN238/16-1) for funding. This work used the Extreme Science and Engineering Discovery Environment (XSEDE), which is supported by U.S. National Science Foundation Grant Number OCI-1053575. J. Friedrich is grateful to Dr. A. Zabula and the Schelter Group for their support and hospitality during his visit. Special thanks go to Dr. A. Berkefeld and F. Koch, as well as N. Mews and Prof. Dr. B. Speiser for helpful discussions regarding the electrochemical studies. We also thank Dr. K. Eichele and K. Strohmaier for technical assistance with the VT ^{1}H NMR spectroscopy experiments.

Keywords: cerium • electrochemistry • hemilability • redox • siloxide

References

1 N. A. Piro, J. R. Robinson, P. J. Walsh and E. J. Schelter, *Coord. Chem. Rev.*, 2014, **260**, 21-36.

2 J. R. Levin, W. L. Dorfner, A. X. Dai, P. J. Carroll and E. J. Schelter, *Inorg. Chem.*, 2016, **55**, 12651-12659.

3 A. Gulino, M. Casarin, V. P. Conticello, J. G. Gaudiello, H. Mauermann, I. Fragala and T. J. Marks, *Organometallics*, 1988, **7**, 2360-2364.
4 J. Xu, E. Radkov, M. Ziegler and K. N. Raymond, *Inorg. Chem.*, 2000, **39**, 4156-4164.
5 T. Behrsing, A. M. Bond, G. B. Deacon, C. M. Forsyth, M. Forsyth, K. J. Kamble, B. W. Skelton and A. H. White, *Inorg. Chim. Acta*, 2003, **352**, 229-237.
6 Y. Bian, J. Jiang, Y. Tao, M. T. M. Choi, R. Li, A. C. H. Ng, P. Zhu, N. Pan, X. Sun, D. P. Arnold, Z.-Y. Zhou, H.-W. Li, T. C. W. Mak and D. K. P. Ng, *J. Am. Chem. Soc.*, 2003, **125**, 12257-12267.
7 J.-W. Zhang, P.-F. Yan, G.-M. Li, B.-Q. Liu and P. Chen, *J. Organomet. Chem.*, 2010, **695**, 1493-1498.
8 E. M. Broderick, P. S. Thuy-Boun, N. Guo, C. S. Vogel, J. Sutter, J. T. Miller, K. Meyer and P. L. Diaconescu, *Inorg. Chem.*, 2011, **50**, 2870-2877.
9 C. Chen, H. Chen, P. Yan, G. Hou and G. Li, *Inorg. Chim. Acta*, 2013, **405**, 182-187.
10 J. W. Buchler and T. Dippell, Eur. *J. Inorg. Chem.*, 1998, 445-449.
11 F. Ortu, J. Liu, M. Burton, J. M. Fowler, A. Formanuik, M.-E. Boulon, N. F. Chilton and D. P. Mills, *Inorg. Chem.*, 2017, **56**, 2496-2505.
12 D. Lionetti, V. W. Day and J. D. Blakemore, *Dalton Trans.*, 2017, **46**, 11779-11789.
13 E. N. Tarakanova, O. A. Levitskiy, T. V. Magdesieva, P. A. Tarakanov, V. Pushkarev and L. G. Tomilova, *New J. Chem.*, 2015, **39**, 5797-5804.
14 G.-C. Wang, Y.-M. So, K.-L. Wong, K.-C. Au-Yeung, H. H. Y. Sung, I. D. Williams and W.-H. Leung, *Chem. - Eur. J.*, 2015, **21**, 16126-16135.
15 J. R. Robinson, P. J. Carroll, P. J. Walsh and E. J. Schelter, *Angew. Chem. Int. Ed.*, 2012, **51**, 10159-10163.
16 J. R. Robinson, Z. Gordon, C. H. Booth, P. J. Carroll, P. J. Walsh and E. J. Schelter, *J. Am. Chem. Soc.*, 2013, **135**, 19016-19024.
17 S. F. Haddad and K. N. Raymond, *Inorg. Chim. Acta*, 1986, **122**, 111-118.
18 B. D. Mahoney, N. A. Piro, P. J. Carroll and E. J. Schelter, *Inorg. Chem.*, 2013, **52**, 5970-5977.
19 A. C. Behrle, J. R. Levin, J. E. Kim, J. M. Drewett, C. L. Barnes, E. J. Schelter and J. R. Walensky, *Dalton Trans.*, 2015, **44**, 2693-2702.
20 J. E. Kim, P. J. Carroll and E. J. Schelter, *Chem. Commun.*, 2015, 51, 15047-15050.
21 J. E. Kim, P. Carroll and E. J. Schelter, *New J. Chem.*, 2015, **39**, 6076-6084.
22 J. R. Levin, W. L. Dorfner, P. Carroll and E. J. Schelter, *Chem. Sci.*, 2015, **6**, 6925-6934.
23 L. A. Solola, P. J. Carroll and E. J. Schelter, *J. Organomet. Chem.*, 2017, **857**, 5-9.
24 J. A. Bogart, C. A. Lippincott, P. J. Carroll, C. H. Booth and E. J. Schelter, *Chem. - Eur. J.*, 2015, **21**, 17850-17859.
25 J. A. Bogart, A. J. Lewis, S. A. Medling, N. A. Piro, P. J. Carroll, C. H. Booth and E. J. Schelter, *Inorg. Chem.*, 2013, **52**, 11600-11607.
26 H. Yin, A. J. Lewis, P. Carroll and E. J. Schelter, *Inorg. Chem.*, 2013, **52**, 8234-8243.
27 K. C. Armstrong, S. Hohloch, T. D. Lohrey, R. A. Zarkesh, J. Arnold and M. R. Anstey, *Dalton Trans.*, 2016, **45**, 18653-18660.
28 L. A. Solola, A. V. Zabula, W. L. Dorfner, B. C. Manor, P. J. Carroll and E. J. Schelter, *J. Am. Chem. Soc.*, 2017, **139**, 2435-2442.
29 M. K. Assefa, G. Wu and T. W. Hayton, *Chem. Sci.*, 2017, **8**, 7873-7878.
30 T. A. Pham, A. B. Altman, S. C. E. Stieber, C. H. Booth, S. A. Kozimor, W. W. Lukens, D. T. Olive, T. Tyliszczak, J. Wang, S. G. Minasian and K. N. Raymond, *Inorg. Chem.*, 2016, **55**, 9989-10002.
31 U. J. Williams, B. D. Mahoney, A. J. Lewis, P. T. DeGregorio, P. J. Carroll and E. J. Schelter, *Inorg. Chem.*, 2013, **52**, 4142-4144.
32 R. P. Kelly, L. Maron, R. Scopelliti and M. Mazzanti, *Angew. Chem. Int. Ed.*, 2017, **56**, 15663-15666.
33 C. M. Kotyk, M. E. Fieser, C. T. Palumbo, J. W. Ziller, L. E. Darago, J. R. Long, F. Furche and W. J. Evans, *Chem. Sci.*, 2015, **6**, 7267-7273.
34 P. B. Hitchcock, M. F. Lappert, L. Maron and A. V. Protchenko, *Angew. Chem. Int. Ed.*, 2008, **47**, 1488-1491.
35 U. J. Williams, P. J. Carroll and E. J. Schelter, *Inorg. Chem.*, 2014, **53**, 6338-6345.
36 N. G. Connelly and W. E. Geiger, *Chem. Rev.*, 1996, **96**, 877-910.
37 R. J. LeSuer and W. E. Geiger, *Angew. Chem.*, 2000, **112**, 254-256; *Angew. Chem. Int. Ed.*, 2000, **39**, 248-250.
38 H. B. Lee, J. A. Bogart, P. J. Carroll and E. J. Schelter, *Chem. Commun.*, 2013, **50**, 5361-5363.
39 U. J. Williams, D. Schneider, W. L. Dorfner, C. Maichle-Mössmer, P. J. Carroll, R. Anwander and E. J. Schelter, *Dalton Trans.*, 2014, **43**, 16197-16206.
40 W. L. Dorfner, P. J. Carroll and E. J. Schelter, *Dalton Trans.*, 2014, **43**, 6300-6303.
41 M. Gregson, E. Lu, D. P. Mills, F. Tuna, E. J. L. McInnes, C. Hennig, A. C. Scheinost, J. McMaster, W. Lewis, A. J. Blake, A. Kerridge and S. T. Liddle, *Nat. Commun.*, 2017, **8**, 14137.
42 J. R. Robinson, Y. Qiao, J. Gu, P. J. Carroll, P. J. Walsh and E. J. Schelter, *Chem. Sci.*, 2016, **7**, 4537-4547.
43 P. L. Arnold, I. J. Casely, S. Zlatogorsky and C. Wilson, *Helv. Chim. Acta*, 2009, **92**, 2291-2303.
44 A. R. Crozier, A. M. Bienfait, C. Maichle-Mössmer, K. W. Törnroos and R. Anwander, *Chem. Commun.*, 2013, **49**, 87-89.
45 D. Werner, G. B. Deacon, P. C. Junk and R. Anwander, *Chem. - Eur. J.*, 2014, **20**, 4426-4438.
46 D. Schneider, T. Spallek, C. Maichle-Mössmer, K. W. Törnroos and R. Anwander, *Chem. Commun.*, 2014, **50**, 14763-14766.
47 P. Dröse, A. R. Crozier, S. Lashkari, J. Gottfriedsen, S. Blaurock, C. G. Hrib, C. Maichle-Mössmer, C. Schädle, R. Anwander and F. T. Edelmann, *J. Am. Chem. Soc.*, 2010, **132**, 14046-14047.
48 I. J. Casely, S. T. Liddle, A. J. Blake, C. Wilson and P. L. Arnold, *Chem. Commun.*, 2007, 5037-5039.
49 P. S. Gradeff, K. Yunlu, T. J. Deming, J. M. Olofson, J. W. Ziller and W. J. Evans, *Inorg. Chem.*, 1989, **28**, 2600-2604.
50 G.-C. Wang, H. H. Y. Sung, I. D. Williams and W.-H. Leung, *Inorg. Chem.*, 2012, **51**, 3640-3647.
51 Y. M. So, G. C. Wang, Y. Li, H. H. Sung, I. D. Williams, Z. Lin and W. H. Leung, *Angew. Chem.*, 2014, **126**, 1652-1655; *Angew. Chem. Int. Ed.*, 2014, **53**, 1626-1629.
52 Y.-M. So and W.-H. Leung, *Coord. Chem. Rev.*, 2016, **340**, 172-197.
53 J. Friedrich, C. Maichle-Mössmer and R. Anwander, *Chem. Commun.*, 2017, **53**, 12044-12047.
54 G. Lapadula, M. P. Conley, C. Copéret and R. A. Andersen, *Organometallics*, 2015, **34**, 2271-2277.
55 a) C. Camp, J. Pécaut and M. Mazzanti, *J. Am. Chem. Soc.*, 2013, **135**, 12101-12111; b) C. Camp, C. E. Kefalidis, J. Pécaut, L. Maron and M. Mazzanti, *Angew. Chem.*, 2013, **125**, 12878-12882; *Angew. Chem. Int. Ed.*, 2013, **52**, 12646 –12650.
56 A. Fischbach, G. Eickerling, W. Scherer, E. Herdtweck and R. Anwander, *Z. Naturforsch., B: J. Chem. Sci.*, 2004, **59**, 1353-1364.
57 P. T. Wolczanski, *Polyhedron*, 1995, **14**, 3335-3362.
58 C. Krempner, *Eur. J. Inorg. Chem.*, 2011, 1689-1698.
59 R. P. Kelly, M. Falcone, C. A. Lamsfus, R. Scopelliti, L. Maron, K. Meyer, M. and Mazzanti, *Chem. Sci.*, 2017, **8**, 5319-5328.

60 J. Andrez, J. Pécaut, P.-A. Bayle and M. Mazzanti, *Angew. Chem.*, 2014, **126**, 10616-10620; *Angew. Chem. Int. Ed.*, 2014, **53**, 10448-10452.
61 K. W. Terry, K. Su, T. Don Tilley and A. L. Rheingold, *Polyhedron*, 1998, **17**, 891-897.
62 S. N. König, C. Maichle-Mössmer, K. W. Törnroos and R. Anwander, *Z. Naturforsch., B: J. Chem. Sci.*, 2014, **69**, 1375.
63 R. P. Kelly, M. Falcone, C. A. Lamsfus, R. Scopelliti, L. Maron, K. Meyer and M. Mazzanti, *Chem. Sci.*, 2017, **8**, 5319-5328.
64 a) K. Izutsu, in *Electrochemistry in Nonaqueous Solutions*, Wiley-VCH Verlag GmbH & Co. KGaA, 2003; b) P. Zanello, *Inorganic Electrochemistry : Theory, Practice and Application*, The Royal Society of Chemistry Cambridge, 2003.
65 G. Inzelt, in *Handbook of Reference Electrodes*, eds. G. Inzelt, A. Lewenstam and F. Scholz, Springer Berlin Heidelberg, Berlin, Heidelberg, 2013, 14, 331-332.
66 a) O. Johansson, L. O. Johannissen and R. Lomoth, *Chem. - Eur. J.*, 2009, **15**, 1195-1204; b) Lomoth, R., *Antioxid. Redox Signaling*, 2012, **19**, 1803-1814.
67 R. Shannon, *Acta Cryst.*, 1976, **A32**, 751-767.
68 D. P. Fairlie, Y. Ilan and H. Taube, *Inorg. Chem.*, 1997, **36**, 1029-1037.
69 A. Tomita and M. Sano, *Inorg. Chem.*, 1994, **33**, 5825-5830.
70 F. Koch, A. Berkefeld, H. Schubert and C. Grauer, *Chem. - Eur. J.*, 2016, **22**, 14640-14647.
71 U. Kilimann, R. Herbst-Irmer, D. Stalke and F. T. Edelmann, *Angew. Chem. Int. Ed.*, 1994, **33**, 1618-1621.
72 H. Fang, B. E. Cole, Y. Qiao, J. A. Bogart, T. Cheisson, B. C. Manor, P. J. Carroll and E. J. Schelter, *Angew. Chem.*, 2017, **129**, 13635-13639; *Angew. Chem. Int. Ed.*, 2017, **56**, 13450-13454.
73 I. Dance, *Inorg. Chem.*, 2006, **45**, 5084-5091.
74 L. Vivier and D. Duprez, *ChemSusChem*, 2010, **3**, 654-678.
75 N. Pal, E.-B. Cho, A. K. Patra and D. Kim, *ChemCatChem*, 2016, **8**, 285-303.
76 D. C. Bradley, J. S. Ghotra and F. A. Hart, *J. Chem. Soc., Dalton Trans.*, 1973, 1021.
77 J. Barry, J. G. H. Du Preez, E. Els, H. E. Rohwer and P. J. Wright, *Inorg. Chim. Acta*, 1981, **53**, L17-L18.
78 M. J. Frisch, G. W. Trucks, H. B. Schlegel, G. E. Scuseria, M. A. Robb, J. R. Cheeseman, G. Scalmani, V. Barone, B. Mennucci, G. A. Petersson, H. Nakatsuji, M. Caricato, X. Li, H. P. Hratchian, A. F. Izmaylov, J. Bloino, G. Zheng, J. L. Sonnenberg, M. Hada, M. Ehara, K. Toyota, R. Fukuda, J. Hasegawa, M. Ishida, T. Nakajima, Y. Honda, O. Kitao, H. Nakai, T. Vreven, J. Montgomery, J. A., J. E. Peralta, F. Ogliaro, M. Bearpark, J. J. Heyd, E. Brothers, K. N. Kudin, V. N. Staroverov, R. Kobayashi, J. Normand, K. Raghavachari, A. Rendell, J. C. Burant, S. S. Iyengar, J. Tomasi, M. Cossi, N. Rega, J. M. Millam, M. Klene, J. E. Knox, J. B. Cross, V. Bakken, C. Adamo, J. Jaramillo, R. Gomperts, R. E. Stratmann, O. Yazyev, A. J. Austin, R. Cammi, C. Pomelli, J. W. Ochterski, R. L. Martin, K. Morokuma, V. G. Zakrzewski, G. A. Voth, P. Salvador, J. J. Dannenberg, S. Dapprich, A. D. Daniels, Ö. Farkas, J. B. Foresman, J. V. Ortiz, J. Cioslowski and D. J. Fox, *Gaussian 09, Revision A.02*, Gaussian, Inc., Wallingford CT, 2009.
79 M. Dolg, H. Stoll and H. Preuss, *J. Chem. Phys.*, 1989, **90**, 1730-1734.
80 A. V. Marenich, J. Ho, M. L. Coote, C. J. Cramer and D. G. Truhlar, *PCCP*, 2014, **16**, 15068-15106.
81 S. I. Gorelsky and A. B. P. Lever, *J. Organomet. Chem.*, 2001, **635**, 187-196.
82 S. I. Gorelsky, version 6.5, AOMix: Program for Molecular Orbital Analysis, http://www.sg-chem.net/, University of Ottawa, 2011.
83 G. A. Zhurko, D. A. Zhurko, , ChemCraft v1.6, http://chemcraftprog.com/.
84 A. E. Reed, R. B. Weinstock and F. Weinhold, *J. Chem. Phys.*, 1985, **83**, 735-746.5.
85 COSMO, version 1.61, Bruker AXS Inc., Madison, WI, 2012.
86 APEX 2, version 2012.10_0, Bruker AXS Inc., Madison, WI, 2012.
87 APEX 3, version 2016.5-0, Bruker AXS Inc., Madison, WI, 2016.
88 SAINT, version 7.99A, Bruker AXS Inc., Madison, WI, 2010.
89 SAINT, version 8.37A, Bruker AXS Inc., Madison, WI, 2015.
90 G. M. Sheldrick, SADABS, version 2012/1, Bruker AXS Inc., Madison, WI, 2012.
91 SADABS: L. Krause, R. Herbst-Irmer, G. M. Sheldrick and D. Stalke, *J. Appl. Cryst.*, 2015, **48**, 3.
92 G. Sheldrick, *Acta Crystallogr. Sect. A: Found. Crystallogr.*, 2008, **64**, 112-122.
93 C. B. Hübschle, G. M. Sheldrick and B. Dittrich, *J. Appl. Crystallogr.*, 2011, **44**, 1281-1284.
94 L. Farrugia, *J. Appl. Crystallogr.*, 1997, **30**, 565-566.
95 POV-Ray, version 3.6, http://www.povray.org/, Williamstown, Victoria, Australia, Persistence of Vision Pty. Ltd., http://www.povray.org/, 2004.

Graphical contents entry

Redox-enhanced hemilability of the tris(*tert*-butoxy)siloxy ligand at cerium†

Jochen Friedrich, Yusen Qiao, Cäcilia Maichle-Mössmer, Eric J. Schelter* and Reiner Anwander*

Combined structural/electrochemical/computational studies of ceric $Ce[OSi(OtBu)_3]_4$ and cerous $[Ce\{OSi(OtBu)_3\}_4][K(2.2.2\text{-crypt})]$ suggest a redox-modulated coordination switch of the tris(*tert*-butoxy)siloxy ligand.